Structural Relaxation of Amorphous Silicon Carbide

Manabu Ishimaru,[1] In-Tae Bae,[2] Yoshihiko Hirotsu,[1] Syo Matsumura,[3] and Kurt E. Sickafus[4]

[1]*The Institute of Scientific and Industrial Research, Osaka University, Osaka 567-0047, Japan*

[2]*Department of Materials Science and Engineering, Osaka University, Osaka 565-0871, Japan*

[3]*Department of Applied Quantum Physics and Nuclear Engineering and Department of Energy Science and Engineering, Kyushu University, Fukuoka 812-8581, Japan*

[4]*Materials Science and Technology Division, Los Alamos National Laboratory, Los Alamos, New Mexico 87545*

(Received 12 April 2002; published 12 July 2002)

We have examined amorphous structures of silicon carbide (SiC) using both transmission electron microscopy and a molecular-dynamics approach. Radial distribution functions revealed that amorphous SiC contains not only heteronuclear (Si-C) bonds but also homonuclear (Si-Si and C-C) bonds. The ratio of heteronuclear to homonuclear bonds was found to change upon annealing, suggesting that structural relaxation of the amorphous SiC occurred. Good agreement was obtained between the simulated and experimentally measured radial distribution functions.

DOI: 10.1103/PhysRevLett.89.055502 PACS numbers: 61.43.Dq, 61.14.Lj, 61.82.Fk

Amorphous semiconductor alloys are of technological importance for electronic and optoelectronic device applications. In particular, amorphous silicon carbide (*a*-SiC) has attracted considerable interest because of its outstanding physical properties. To obtain desirable materials properties for device production, knowledge of atomistic structures of *a*-SiC is required. For the amorphous networks formed by different atomic species, not only topological disorder but also chemical disorder should be considered. On the basis of Raman spectroscopy [1–4], x-ray photoelectron spectroscopy [4,5], extended x-ray absorption fine-structure spectroscopy [1,6], Fourier-transform infrared spectroscopy [2,4], and electron diffraction [7], two atomistic structural models have been proposed for *a*-SiC. (See also Ref. [8] for additional experimental results.) Some researchers characterized *a*-SiC networks as highly chemically ordered, consisting of heteronuclear (Si-C) first nearest neighbor bonds [5–7]. *a*-SiC basically consists of the same tetrahedral coordinated units as crystalline SiC, wherein a silicon atom is surrounded approximately by four carbon atoms and vice versa. On the other hand, there is evidence for the formation of homonuclear bonds (Si-Si and C-C bonds) in *a*-SiC [1–4]. Although extensive studies have been carried out on the structural analyses of *a*-SiC, the fundamental nature of short-range order (SRO) in *a*-SiC remains a topic of debate.

In addition to the SRO structures, information on structural relaxation processes is also important in order to obtain an appropriate amorphous structure, since vibrational, thermodynamic, and electronic properties of amorphous semiconductors strongly depend on the SRO structure. As compared to the structural analysis of *a*-SiC, however, investigations of structural relaxation processes in *a*-SiC are limited [2,9]. To date, no diffraction study of structural changes during annealing has been published. In this Letter, we examine the SRO structure of *a*-SiC as well as annealing-induced relaxation processes using transmission electron microscopy (TEM) and molecular-dynamics simulations.

a-SiC films grown by chemical vapor deposition generally contain hydrogen atoms. It is known that amorphous structures as well as structural relaxation processes depend on the hydrogen content [10]. We performed ion irradiation into crystalline SiC to produce pure *a*-SiC. Single crystal wafers of (0001)-oriented 6H-SiC (obtained from Cree, Inc. [11]) were irradiated at room temperature with 150 keV argon (Ar^+) ions to a fluence of 10^{16} cm^{-2}. According to Monte Carlo simulations using the TRIM code (TRIM-90) [12], the maximum concentration of Ar is about 1.5% at this ion fluence. This ion irradiation procedure produces an *a*-SiC layer ~200 nm thick on the surface of the SiC wafers. Some ion-irradiated samples were then annealed at 800 °C for 2 h. Both as-irradiated and annealed samples were analyzed using TEM and electron diffraction techniques. Irradiation-induced microstructures were observed using a JEOL JEM-2010 TEM with an incident electron energy of 200 kV. Atomistic structures of ion-beam-induced amorphous layers were examined by electron diffraction techniques. Halo patterns were recorded on an imaging plate (Eu^{2+}-doped BaFBr). This has a higher sensitivity and a wider dynamic range for electron-beam intensities compared to conventional TEM film [13]. The intensities of the halo pattern were analyzed quantitatively in an imaging plate processor, specifically a digital microluminography FDL 5000 system (Fuji Film). The details of the electron diffraction analysis are described elsewhere [14–16].

Figure 1 shows bright-field images of (a) as-irradiated and (b) 800 °C annealed SiC samples, together with electron diffraction patterns obtained from the topmost layer of the irradiation-induced microstructure. The samples were aligned near a $[10\bar{1}0]$ orientation to obtain the images in Fig. 1. In both samples, a distinct image contrast is

 © 2002 The American Physical Society

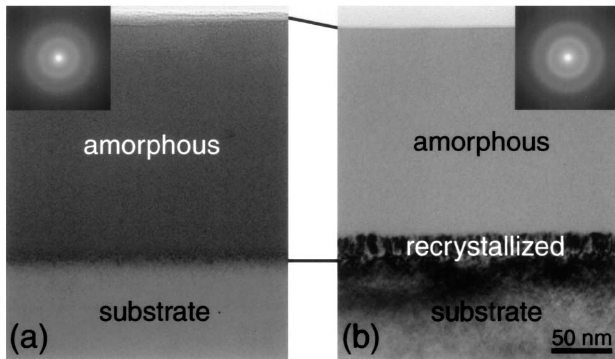

FIG. 1. Cross-sectional bright-field images of as-irradiated and 800 °C annealed samples. The corresponding electron diffraction patterns indicate that the irradiated layer in both samples is completely amorphized.

observed at the topmost layer. High-resolution TEM and electron diffraction observations revealed that the topmost layer is completely amorphous without any crystalline inclusions (except near the amorphous-to-crystalline interfaces). The thickness of the amorphous layer is ~200 nm in Fig. 1(a), while it is ~170 nm in Fig. 1(b). In Fig. 1(b), it is apparent that a recrystallized layer with a width of ~20 nm is formed at the amorphous-to-crystalline interface. It should be noted that when SiC undergoes a crystalline-to-amorphous phase transformation, the density decreases from 3.21 to 2.75 g/cm^3 [17]. Even though this density change is considered, the volume reduction of 30 nm is too large: the amorphous layer itself shrinks in annealing. This result is consistent with previous investigations [17,18].

Information regarding the SRO structures of the irradiation-induced *a*-SiC was obtained from electron diffraction patterns. The incident electron-beam was focused to ~50 nm diameter and the nanobeam electron diffraction patterns were obtained from the center of the amorphous layer. Electron diffracted intensities are highly susceptible to modification by dynamical effects such as multiple scattering. With this in mind, electron diffraction patterns were obtained from TEM sample regions that were as thin as possible. Electron diffraction patterns were obtained using different exposure times, and it was confirmed that intensity profiles are unaffected by exposure time. This indicates that radiation damage of *a*-SiC induced by the electron-beam during diffraction analysis is negligible. From the measured electron diffraction intensity profiles, reduced interference functions, $F(Q)$, were calculated. Figure 2 shows the $F(Q)$ function obtained from the sample annealed at 800 °C (solid line) compared to the $F(Q)$ obtained from the as-irradiated sample (broken line). The measured $F(Q)$ exhibit substantial differences in both the heights and widths of the first and second peaks in F versus Q. These peaks become more pronounced with annealing.

Very weak intensity profiles can be recorded up to high scattering angles (as high as $Q \sim 220\ nm^{-1}$), well above

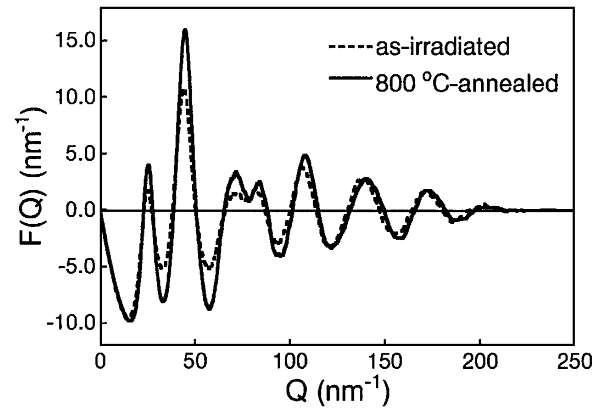

FIG. 2. Comparison of reduced interference functions $F(Q)$ of as-irradiated (broken line) and 800 °C annealed *a*-SiC (solid line).

the background intensity level of the imaging plate. (The scattering vector in reciprocal-lattice space is defined as $Q = 4\pi \sin\theta/\lambda$, where θ and λ are the scattering half angle and the electron wavelength, respectively.) The maximum scattering vector measured in this study is much larger than that measured by previous electron diffraction [7,19] and x-ray diffraction experiments [20]. Consequently, we obtain higher resolution in real-lattice space compared to previous diffraction studies.

Reduced radial distribution functions, $g(r)$, were calculated via Fourier transformation of $F(Q)$. The resulting $g(r)$ are shown in Fig. 3. Also shown in Fig. 3 are the interatomic distances associated with crystalline SiC (marked with arrows in the bottom part of Fig. 3). The first and second nearest neighbors are centered at $0.188(\pm 0.002)$ and 0.307 nm, respectively. These values correspond to the bond lengths of Si-C (the first nearest neighbor) and Si-Si (the second nearest neighbor) in crystalline SiC. In addition to these peaks, subpeaks appear on

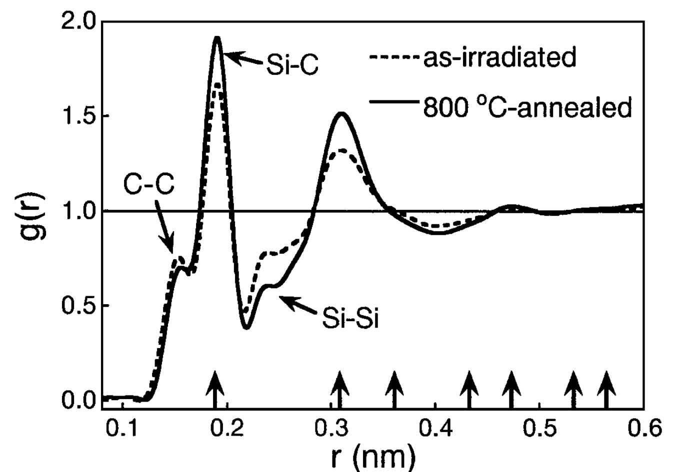

FIG. 3. The experimentally measured reduced radial distribution functions $g(r)$ of as-irradiated (broken line) and 800 °C annealed *a*-SiC (solid line).

either side of the Si-C peak in Fig. 3. The r positions of these peaks, 0.151 and 0.238 nm, can be assigned to C-C and Si-Si bond lengths [8,21], respectively. This suggests that a-SiC networks contain not only heteronuclear bonds but also homonuclear bonds. The C-C subpeak at 0.151 nm is comparable with the nearest neighbor distances found in graphite (0.143 nm) and diamond (0.155 nm). This result is consistent with previous experimental results obtained by Fourier-transformed infrared spectroscopy and Raman spectroscopy [4] and suggests the existence of sp^2- and sp^3-bonded carbon atoms in a-SiC. The $g(r)$ obtained here is in good agreement with molecular-dynamics simulations of a-SiC quenched from the liquid [8,21] or produced by ion irradiation [22].

Substantial changes in the $g(r)$ were observed during annealing. The major differences between as-irradiated and annealed a-SiC are apparent within the second coordination shell (< 0.4 nm). Only small differences are observed beyond the second peak. This implies that the largest variations in atomic configurations are in the SRO range. The locations of the first and second nearest neighbor peaks are not affected by annealing. The peak associated with the heteronuclear Si-C bond (0.188 nm) becomes more pronounced, whereas the peaks associated with homonuclear bonds (0.151 and 0.238 nm) decrease during annealing. It should be noted that Si-Si bonds at 0.238 nm decrease more rapidly than C-C bonds at 0.151 nm. This is attributed to the difference of the bond energy between Si-Si (2.32 eV/bond) and C-C (3.68 eV/bond). These diffraction analysis results are the first to provide information regarding structural changes due to relaxation of a-SiC.

Void-free amorphous silicon produced by ion irradiation exhibits almost the same density as crystalline silicon, and the density is unchanged by annealing. On the other hand, Höfgen *et al.* [18] examined the annealing behavior of a-SiC using profilometry and x-ray diffraction and observed large volume reduction (so-called "densification") of a-SiC prior to crystallization. A previous investigation reported that the annihilation of point defects leads to substantial densification [17]. In addition to this, the difference of annihilation speed between Si-Si and C-C homonuclear bonds (as seen in Fig. 3) may play an important role in explaining the large volume changes in a-SiC.

Structural changes of a-SiC during annealing were also investigated by molecular-dynamics simulations using Tersoff interatomic potential [23]. The a-SiC networks were prepared by computational procedures similar to those used in previous studies on amorphous silicon [24–26]. Figure 4 shows $g(r)$ for unrelaxed (broken line) and relaxed a-SiC (solid line). Note that the atomic scattering factors are not weighted in Fig. 4, so the $g(r)$ in Fig. 4 indicates only qualitative trends. The unrelaxed a-SiC was generated by quenching molten SiC from 4500 to 300 K with a cooling rate of 10^{12} K/s, while the relaxed a-SiC was prepared by annealing the unrelaxed a-SiC at 2000 K for 10 ns. Again, it was confirmed that the peak for Si-C

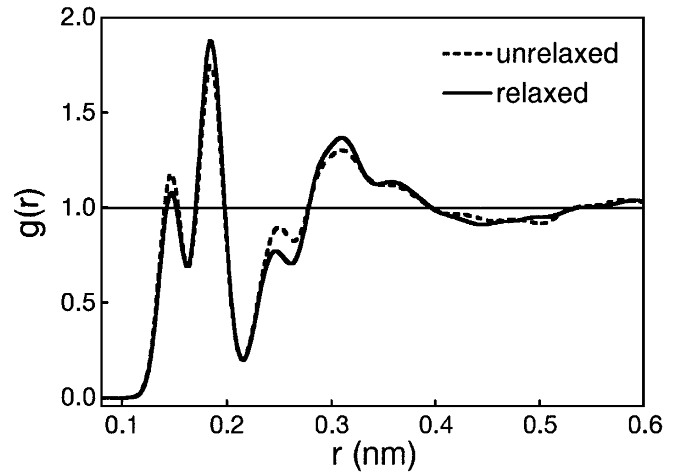

FIG. 4. Reduced radial distribution functions calculated by molecular-dynamics simulations. The unrelaxed a-SiC network (broken line) was generated by quenching liquid SiC, while the relaxed a-SiC (solid line) were prepared by annealing the unrelaxed a-SiC.

heteronuclear bonds increases, while the subpeaks for C-C and Si-Si homonuclear bonds decrease after annealing. This reproduces qualitatively the $g(r)$ obtained experimentally (Fig. 3). As mentioned previously, in earlier studies a-SiC was interpreted as a heteronuclear-bonded random tetrahedral network [5–7]. Our present study shows that the ratio of homonuclear to heteronuclear bonds is altered upon annealing. Chemical order develops as annealing progresses. The highly chemically ordered a-SiC may correspond to a fully relaxed state of a-SiC.

In summary, experimentally obtained radial distribution functions, $g(r)$, reveal the existence of C-C and Si-Si bonds in the first coordination shell of a-SiC. This suggests that a-SiC possesses not only heteronuclear but also homonuclear bonds. Substantial changes in $g(r)$ were observed during annealing of a-SiC. Significant changes in SRO configurations occur within the second coordination shell, while only small differences are observed at larger interatomic distances. The peaks associated with heteronuclear bonds become more pronounced during annealing, while peaks corresponding to homonuclear bonds simultaneously decrease. This behavior was also confirmed by molecular-dynamics simulations.

We thank J. R. Tesmer, C. J. Wetteland, and J. A. Valdez for their assistance with ion implantations and T. Ohkubo for his development of the computer code for electron diffraction analysis. This work was sponsored by the U.S. Department of Energy (DOE), Office of Basic Sciences, Division of Materials Sciences, and the Center of Excellence (COE) program and Special Coordination Fund for Promoting Science and Technology on "Nanohetero Metallic Materials" from the Science and Technology Agency and a Grant-in-Aid for Scientific Research from the Ministry of Education, Science, Sports and Culture, Japan.

[1] W. Bolse, Nucl. Instrum. Methods Phys Res., Sect. B **148**, 83 (1999).
[2] P. Mélinon, P. Kéghélian, A. Perez, J.L. Rousset, A.M. Cadrot, A. Malhomme, A.J. Renouprez, and F.J. Cadete Santos Aires, Philos. Mag. A **80**, 143 (2000).
[3] P. Musumeci, F. Roccaforte, and R. Reitano, Europhys. Lett. **55**, 674 (2001).
[4] C. Serre, L. Calvo-Barrio, A. Pérez-Rodríguez, A. Romano-Rodríguez, J.R. Morante, Y. Pacaud, R. Kögler, V. Heera, and W. Skorupa, J. Appl. Phys. **79**, 6907 (1996).
[5] T. Takeshita, Y. Kurata, and S. Hasegawa, J. Appl. Phys. **71**, 5395 (1992).
[6] A.E. Kaloyeros, R.B. Rizk, and J.B. Woodhouse, Phys. Rev. B **38**, 13 099 (1988).
[7] J. Bentley, P. Angelini, A.P. Gove, P.S. Sklad, and A.T. Fisher, Inst. Phys. Conf. Ser. **98**, 107 (1989).
[8] F. Finochhi, G. Galli, M. Parrinello, and C.M. Bertoni, Phys. Rev. Lett. **68**, 3044 (1992).
[9] P. Musumeci, R. Reitano, L. Calcagno, F. Roccaforte, A. Makhtari, and M.G. Grimaldi, Philos. Mag. B **76**, 323 (1997).
[10] P. Musumeci, L. Calcagno, and A. Makhtari, Mater. Sci. Eng. A **253**, 296 (1998).
[11] Cree, Inc., 4600 Silicon Drive, Durham, NC 27703.
[12] J.F. Ziegler, J.P. Biersack, and U. Littmark, *The Stopping and Range of Ions in Solids* (Pergamon, New York, 1985).
[13] N. Mori, T. Oikawa, T. Katoh, J. Miyahara, and Y. Harada, Ultramicroscopy **25**, 195 (1988).
[14] T. Ohkubo, T. Hiroshima, Y. Hirotsu, A. Inoue, and T. Oikawa, Mater. Trans. JIM **41**, 1385 (2000).
[15] Y. Hirotsu, M. Ishimaru, T. Ohkubo, T. Hanada, and M. Sugiyama, J. Electron Microsc. **50**, 435 (2001).
[16] M. Ishimaru, Y. Hirotsu, I.V. Afanasyev-Charkin, and K.E. Sickafus, J. Phys. Condens. Matter **14**, 1237 (2002).
[17] V. Heera, F. Prokert, N. Schell, H. Seifarth, W. Fukarek, M. Voelskow, and W. Skorupa, Appl. Phys. Lett. **70**, 3531 (1997).
[18] A. Höfgen, V. Heera, F. Eichhorn, and W. Skorupa, J. Appl. Phys. **84**, 4769 (1998).
[19] A. Sproul, D.R. McKenzie, and D.J.H. Cookayne, Philos. Mag. B **54**, 113 (1986).
[20] C. Meneghini, S. Pascarelli, F. Boscherini, S. Mobilio, and F. Evangelisti, J. Non-Cryst. Solids **137/138**, 75 (1991).
[21] D. Mura, L. Colombo, R. Bertoncini, and G. Mula, Phys. Rev. B **58**, 10 357 (1998).
[22] F. Gao and W.J. Weber, J. Appl. Phys. **89**, 4275 (2001).
[23] The validity of the Tersoff potential for covalent materials is described in the following articles: M. Ishimaru, K. Yoshida, and T. Motooka, Phys. Rev. B **53**, 7176 (1996); M. Ishimaru, K. Yoshida, T. Kumamoto, and T. Motooka, Phys. Rev. B **54**, 4638 (1996).
[24] M. Ishimaru, S. Munetoh, and T. Motooka, Phys. Rev. B **56**, 15 133 (1997).
[25] M. Ishimaru, J. Phys. Condens. Matter **13**, 4181 (2001).
[26] M. Ishimaru, J. Appl. Phys. **91**, 686 (2002).